厚生労働科学研究費補助金

エイズ対策研究事業

計算機を活用したHIVの薬剤耐性評価

平成１５年度～１６年度　総合研究報告書

主任研究者　　星野　忠次

平成１７（２００５）年　３月

厚生労働科学研究費補助金（エイズ対策研究事業）
「計算機を活用したＨＩＶの薬剤耐性評価」
平成１５～１６年度　総合研究報告書

<p align="center">目　　次</p>

計算機を活用したＨＩＶの薬剤耐性評価

主任研究者　星野忠次（千葉大学大学院薬学研究院　助教授）

研究要旨　　抗エイズ薬に対する HIV 感染患者の個別ウィルスの薬剤耐性度を、計算機を利用して評価するための技術開発を行った。耐性評価プログラムの開発を星野(千葉大学薬学研究院)が行い、実際の計算解析を畑(千葉大学薬学研究院)が遂行した。計算結果と既存の実験的検査結果との照合を杉浦(国立感染症研究所エイズ研究センター)が担当し、臨床データとの比較を佐藤(千葉大学医学部附属病院)が行った。抗エイズ薬に対する薬剤耐性を評価するためのソフトウェアは、計算手続きと親和性評価に大別できる。計算手続きとしては、ウィルスの塩基配列から薬剤と変異型酵素複合体のモデルを作成する部分、計算準備としてモデルへ生体内条件を適用する部分、生体内シミュレーションを実行して構造平衡化を計算する部分、最終的に結合エネルギーや構造変化ならびにゆらぎ解析を行う部分を構築した。親和性評価としては、結合エネルギー解析、構造変化解析、ならびにゆらぎ解析を開発し、良く知られたアミノ酸変異を持つ菌株に適用し、これらが実験的に知られている薬剤耐性評価と整合性のあることを確認した。薬剤－酵素間の親和性に関して従来の計算方法では評価が困難であった微少な違いを、再現性良く求める手法が開発できた。既にフェノタイプ検査が実施された臨床検体由来の菌株１０検体について、この方法を適用したところ、複数の評価方法を組合せることで、既存の実験データと計算値との間に良い整合性が見られるようになった。検証例を増やすことが今後の課題である。以上の作業を、半自動的にできるようにプログラムの整理を行い、計算実行の効率化を図った。

　　　分担研究者
畑　晶之（千葉大学大学院薬学研究院　助手）
佐藤武幸（千葉大学医学部附属病院　感染症管理
　　　　治療部長、助教授）
杉浦　亙（国立感染症研究所、エイズ研究センタ
　　　　ー　第２研究グループ長）
　　　協力研究者
横幕能行（千葉大学医学部附属病院　助手）
布施　晃（国立感染症研究所　血液・安全性研究
　　　　部長）

A．研究目的

　抗 HIV 薬は長期にわたる投与を余儀なくされるため、ウィルスが薬剤抵抗性を獲得し、耐性ウィルスが発生してしまうことが、HIV 感染症治療では深刻な問題となっている。そこで HIV 感染患者に薬を投与する前に、予め薬剤耐性検査を行うことが、抗 HIV 療法をより充実させるために重要である。これに対応して、HIV のジェノタイプとフェノタイプを迅速に決める検査技術が開発され、抗 HIV 療法の一環として、耐性検査を行うことが現実のものとなっている。

　本研究では、ジェノタイプ検査やフェノタイプ検査に並ぶ新しい薬剤耐性検査法として、「コンピューテーショナル検査」を提案している。この技術の実現に向け、計算手法の開拓を中心に開発を推進してきた。本研究の目標は、計算機を駆使した理論的方法により、国内で認可されている抗 HIV 薬のうち、個々の患者にとって最も適した薬剤を選択できる技術を確立することである。

　仮に、患者ごとに最も適した薬剤を事前に選択することができるようになれば、一般的な経験則

による不用意な薬剤投与と薬剤耐性発生を回避することができ、患者の負担を軽減することができる。さらに、不必要なウィルス耐性発生を抑えられるので、使用可能な薬剤の選択を広げられ、よりよい治療効果を期待できる。本研究班は、多様な変異 HIV 株に特異的に有効な治療薬を、コンピュータシミュレーションを用いて予測することで、HIV 感染患者の薬物治療を効率的なものとすることを目指している。

B．研究方法

患者ごとに異なる酵素の構造変異を計算機内で再現し、抗エイズ薬への抵抗性を算出するシステムを構築するために、方法論の開拓ならびに実験的知見との整合性確認という2つの観点より、以下に示す項目に分けて研究を進めた。特に本研究では、計算機で評価された検査結果に、高い信頼性があるか、十分に新規の医療技術として臨床に応用できるものかを確認することが、最大のポイントである。そこで、従来のジェノタイプ検査やフェノタイプ検査と照らし合わせて、計算機で算出した値が、実験的方法と整合性があるかを詳細に調べている。

<u>ソフトウェア開発（方法論の開拓）</u>
(項目1) 計算評価法改良と計算機プログラムの作成
(項目2) 計算の迅速化に向けた取り組み
計算を実行する際のソフトウェアとして、(1)計算手続きをルーチン化し、共通の計算を遂行できるようにすること、(2)親和性評価の精度の向上を図り計算による予測の信頼性を確保すること、が必要になる。(1)計算手続きのルーチン化は、分子シミュレーションをHIV-1プロテアーゼと阻害剤の結合に限定することで、シミュレーションの手続きの共通化できる部分をプログラム化し、計算の効率化を図る。(2)親和性評価法の開拓では、実験で測定されたフェノタイプ検査の測定値と計算で算出される値を比較して、有効性の確認を行う必要がある。実験測定値としては、既にジ

ェノタイプで耐性になると知られている一つの変異を持った単純な実験室株での測定値を利用する。具体的には、D30N や L90M や N88D ならびに Wild タイプのプロテアーゼとこれに阻害剤の Nelfinavir が結合した系を利用する。計算手法として、(a)薬と標的酵素の結合エネルギーから評価する方法、(b)反応ポケットの歪みと反応ポケットの体積の増加を測定する方法、(c)接合面のゆらぎ具合から推定する方法の3つを試みた。

<u>既存データとの比較（整合性確認）</u>
(項目1) フェノタイプ検査が既知のデータを、照合例として使用
(項目2) 変異情報から、検体固有の酵素を計算機内で仮想的に作成し、薬剤-変異酵素結合構造を構築
(項目3) 薬剤と酵素の結合力の算出と薬剤抵抗性の評価
(項目4) 計算機算出値と実験データとの比較
分担研究者(杉浦)の蓄積している解析データの中より、検査会社(Virco)によりフェノタイプ検査の行われた検体について、計算機解析を実行し、これとフェノタイプ検査との比較を行う。

<u>臨床データとの比較（整合性確認）</u>
(項目1) 患者からのサンプル採取とウィルス量の測定
(項目2) 国立感染症研究所エイズ研究センターでのサンプルのジェノタイプ検査
(項目3) ジェノタイプ検査、治療経過および計算評価結果を比較
HIV の薬剤耐性評価に関する計算結果と現実系の比較を、次の手順で行う。(1)分担研究者(佐藤)の担当している患者から、倫理審査委員会で審議を経た上で、血液をサンプルとして採取する。同時にCD4細胞数やHIV-RNA量などの臨床上の諸量を測定する。(2)採取されたサンプルは、国立感染症研究所エイズ研究センターに送付する。分担研究者(杉浦)は、通常業務の中でこのサンプルのジェノタイプとフェノタイプ検査を行う。(3)ジェノタイプ検査の際に、DNA シーケンサーにより

読み取られた酵素の変異情報を、主任研究者(星野)に送る。(4) 変異情報から、患者固有の酵素に関して、薬剤-変異酵素結合構造をコンピューター内で構築し、薬剤と酵素との結合親和性から、薬剤抵抗性を評価する。(5)主任研究者からは計算機による薬剤評価をが示される。また、変異によって、著しく薬効が減少したものについて、薬剤抵抗性の注意が示される。(6)ジェノタイプ検査ならびに計算結果のフィードバックを受け、HIV 感染者への治療の中で、この情報を比較検討し、技術の有意性を判断する。

(倫理面への配慮)

患者からの試料採取は、千葉大学大学院医学研究院倫理審査委員会での審議を経て行い、提供者に菌株が実験に利用される旨の説明をして同意を得る。分担研究者(佐藤)以外は、個人識別情報は全く参照できない。コンピューテーショナル検査の実施においては、主任研究者らは患者とは全く接点が無い。

C. 研究結果

ソフトウェア開発

(1)計算手続きのルーチン化

計算を実行し評価するまでに、(A)ウィルスの塩基配列から薬剤と変異型酵素複合体のモデルを作成する部分、(B)計算準備としてモデルへ生体内条件を適用する部分、(C)生体内シミュレーションを実行して構造平衡化を計算する部分、(D)最終的に結合エネルギーや構造変化ならびにゆらぎ解析を行う部分が必要となる。(A)ウィルスの塩基配列から薬剤と変異型酵素複合体のモデルを作成する部分では、SEQ_DETERM というソフトウェアを独自に開発した。これにより塩基配列からアミノ酸配列への変換やPDB ファイルの編集が可能となる。これ以外に、MultiAlignment, Transform, Makeparm などのソフトウェアが開発され、実際に利用している。(B)計算準備としてモデルへ生体内条件を適用する部分では、標準的な市販分子動力学ソフトウェアパッケージであ

る AMBER8 を利用するために、Leap_load_data, res2res などのプログラムが作成された。これを用いて酵素のまわりに溶媒として水分子を発生させ、初期値の絶対零度から生体温度までの昇温を行う。(C)生体内シミュレーションを実行して構造平衡化を計算する部分では、AMBER8 の分子動力学計算を 2n 秒程実行する。このとき Constraint_sander や PiPi_sander という市販ソフトウェアを修正したものが利用される。(D)最終的に結合親和性評価を行う部分では、エネルギーや構造変化ならびにゆらぎ解析を実施する。このために EnergyDiv_sander, binding_surface, pipi-calc, Volume_area, InterFaceFluctuate, SC_calc などのプログラムが作成された。

(2)親和性評価の精度の向上

酵素と薬物の結合親和性を評価するために、(a)結合エネルギー評価、(b)構造変化による評価、(c)接合面のゆらぎ評価の3つの方法が開発され、試みられた。(a)結合エネルギー評価では、結合エネルギーをクーロン相互作用エネルギー、ファンデルワールス相互作用エネルギー、疎水相互作用エネルギー、π-π相互作用エネルギーの 4 つの総和として算出することにした。Wild タイプのプロテアーゼと D30N ならびに N88D 変異体で、この方法を適用したところ、実験から測定された阻害薬物濃度の比の対数値とほぼ線形の相関が得られた。(b)構造変化による評価では、活性残基である Asp25 から Ile50' の距離と Asp25' から Ile50 の距離の差で構造の歪みの程度を測り、Asp25-Ile50'-Asp25'-Ile50 の作る平面の面積により反応ポケット領域の大きさを測る。これは歪みが大きいほどプロテアーゼの安定性には不利であり、また薬剤とプロテアーゼの結合親和性が低くなると、プロテアーゼのフラップ領域の閉じ具合が不良となり、反応ポケット領域の面積が増加するという知見に基づいている。距離差と面積変化を変数として、これに適当な定数値を掛け合わせることで、親和性を評価するプログラムを作成した。Wild タイプのプロテアーゼと L90M な

らびに N88D 変異体で、この方法を適用したところ、実験で測定された変異構造の薬物抵抗性とほぼ線形の相関が得られた。(c)接合面のゆらぎ評価では、ファンデルワールスエネルギーの時間変動をフーリエ変換して、この要素を加え合わせることにより評価を行う。この方法についても、Wild タイプのプロテアーゼと D30N ならびに N88D 変異体に適用したところ、実験から測定された阻害薬物濃度の比の対数値とほぼ線形の相関が得られた。

既存データとの比較

分担研究者(杉浦)の蓄積している解析データの中より、検査会社(Virco)によりフェノタイプ検査の行われた 36 検体について、主任研究者(星野)は分担研究者(畑)と共に計算機解析を始めた。計算が実行しやすいことならびにジェノタイプ検査だけの結果のみでは十分に耐性度が推定できず、本研究で開発するシステムの有用性が高いことから、本研究ではプロテアーゼ阻害剤に絞り研究を進めた。臨床検体から分離された一つの HIV-1 プロテアーゼ株につき、現在国内で認可されている 7 つのプロテアーゼ阻害剤との結合親和性を順次求め、10 検体について計算を実施することができた。

エネルギー評価法では、インジナビル以外では、臨床検体のフェノタイプの耐性検査と計算予測値との整合性が、ある程度、取れるようになった。また特定の 4 検体では、フェノタイプ耐性検査の結果と計算予測値の間に高い相関がみられた。

反応ポケットの構造変化から評価する方法では、10 検体のうち半分程の検体について、臨床検体のフェノタイプ耐性検査の結果と計算予測値との間に良い整合性が見られた。

ゆらぎ評価法では、変異が 1,2 箇所だけの実験室株に対しては、計算値は実験的薬剤感受性と良い相関が見られる。この評価法を抗原・抗体結合に適用した結果も良い推測値を与えることができるようになった。ところが HIV の臨床株に対し

ては満足の行く結果は得られなかった。

以上の結果からさらに解析方法を工夫し、エネルギー評価法方法と構造変化評価方法を組合わせると、計算機によりフェノタイプ耐性検査の結果を、全 10 検体の平均として、相関係数 (S) =0.8 程で予測することができるようになった。

臨床データとの比較

実際の患者サンプルについて、評価を試みた。分担研究者(佐藤:千葉大学医学部付属病院)より、分担研究者(杉浦:国立感染症研究所)に遺伝子変異の解析を依頼して、ジェノタイプ検査を実施した。ジェノタイプ検査をもとに計算機による評価を主任研究者に依頼したが、計算による予測は、まだ完全に信頼性が保証されないとの理由で、提出が見合わされている。但し、患者の薬剤投与履歴とウィルス量変化やウィルス変異の経過を追跡する必要があるので、分担研究者(佐藤)は、国立感染症研究所に検査を依頼して、後の経時的な評価検討のための準備を進めた。

D. 考察

評価を試みた 3 種類の方法のうち、エネルギー評価法と構造変化評価は、検体によっては、フェノタイプの耐性検査との間に十分な整合性を示した。エネルギー評価法で 4 例、構造変化評価法で 6 例が整合性のある結果を与えた。10 検体のうち、エネルギー評価法で整合性の悪かった検体は、構造変化評価法では良好な整合性を示した。また逆に構造変化評価法であまり整合性が良くない検体は、エネルギー評価法で良い整合性を示した。結局、エネルギーと構造変化は相反し、計算評価は相互に補完するので、両者を併用すると予測精度が著しく向上するということが見えてきた。

本研究で開発してきたエネルギー評価法ならびにゆらぎ評価法は、従来、創薬や生物学の分野で標準的に利用されてきた自由エネルギー計算手法 (MMGBSA 法や MMPBSA 法) よりは、信頼性の高い結果を与えている。但し薬物候補のスクリー

4

ニングでの利用とは異なり、臨床における薬剤選択に利用されるには、相当に計算精度を上げる必要がある。HIV-1 プロテアーゼの薬剤に対する感受性変化が2〜3倍変化するのに対し、1kcal/mol 程度のエネルギー変化しかないと言われており、従来の方法では対処しきれない。従って、本研究で開発された計算手法は、精度の面よりかなり有望であると考えている。本研究で開発してきたエネルギー評価ならびにゆらぎ評価のいずれの方法も、十分に長く計算シミュレーションを行うと精度が向上する。

臨床検体ウィルスの遺伝子配列解析では、A, T, G, C に分類できないコドン（例えば R は A または G に対応）も存在する。これは臨床検体には複数の遺伝型を持つウィルスが混在しているためであると考えられる。検体によっては、確定のできないコドンが複数個所あるために、HIV-1 プロテアーゼ遺伝子の全長に対して千通り以上の組み合わせが生じる場合も多々ある。計算ではどれか一つに確定しないとモデルが作成できないので、一旦、全てのアミノ酸配列の組み合わせを作成し、それを比較して一つの配列に絞り込むことを行った。具体的には、重要な変異の有無、電荷の変化、かさ高さの変化などに順位付けを行い、変異が入ったときに野生株から最も大きな影響を及ぼす可能性のあるものが選択されるようにした。これはフェノタイプ検査との不整合の一因となってしまうが、重大なアミノ酸変異を見過ごすことの無いようにとの判断である。実際に検体を用いた評価を実行すると、この絞込みを行ったとしても、フェノタイプ検査の結果と整合性が保てることが判明した。

計算機によるアプローチでも実験と同様に、計算を実行する人により若干方法が異なるので、必ずしも同一の計算値が算出されるとは限らない。そこでなるべく計算の工程を自動化して、誰が計算しても、また計算機を使うことに不慣れな人でも適正な算出値が得られるように工夫をした。

計算機による薬剤耐性評価を行う場合に、コスト の面で実験的なフェノタイプ検査より安価でなくてはならない。計算中では（C）の生体内シミュレーションの実行が最も時間が掛かる。この計算は薬物が変異の入った HIV-1 プロテアーゼに結合したときの生体温度における平衡構造を求めるためのものである。この構造が正確でないと評価の精度は向上しない。この構造を正確に求めるためには計算機シミュレーションは長ければ長いほど信頼性が高くなる。しかし計算時間からの制約から一つのモデルに対して、2n 秒のシミュレーションを行うこととした。この計算を構造がなるべく早く適切なものになるように、計算のはじめにおいて一部の水分子や原子間に束縛を課すなどの工夫をしている。これにより比較的短い時間のうちに適切な構造が得られるようになった。

今回の研究で開発された3つの結合親和性評価方法は、単純な変異しか持たない実験室株については、良好な評価を与えた。多くの臨床由来の検体は十数箇所に渡り変異が入っていることが多い。計算は Wild タイプの薬物—酵素複合体を元に、これに変異を入れる方式で、薬物—変異型酵素複合体のモデル化を行う。従って、アミノ酸変異の箇所が増えるほど、平衡化構造を得られるまでの計算時間が長くなる。計算時間の制約上、計算時間を決めて実行するが、これが臨床由来の検体を取り扱う場合に計算予測精度を下げることが予想される。当面は、計算精度と実用的な計算時間との間の折合いを見つけることも必要かも知れないが、計算機の性能は年々向上しているので、2-3 年後の将来には、自動的に解決され得る問題と思われる。

E. 結論

コンピュータシミュレーションを用いて、抗エイズ薬に対するウィルスの薬剤耐性を予測するという目的を実用に近づけるために、計算手続きと親和性評価に用いるソフトウェアを開発した。計算をルーチン化し、これらが半自動的にできる

ようにプログラムの作成を行い、計算実行の効率化を図った。また、親和性評価に用いる結合エネルギー解析、構造変化解析、ならびにゆらぎ解析を開発し、これらが実験的に知られている薬剤耐性評価と整合性のあることを確認した。従って、薬剤抵抗性評価に用いるソフトウェアの開発には、一定の成果があった。エネルギー評価法では、実験室株ならびにインジナビルを除くプロテアーゼ阻害剤について、一部の検体について、計算機による親和性の算出値と実験による測定値の間の整合性がみられるようになった。構造変化評価法でも、一部の検体に対して良好な整合性を示した。エネルギー評価と構造変化評価は相反し、計算評価は相互に補完する。すなわちエネルギー評価の整合性が高いものは、構造変化評価の整合性が低く、逆にエネルギー計算評価の整合性が低いものは構造変化評価の整合性が高い。従って、両者を併用すると予測精度が著しく向上するということがわかった。今後、評価法をさらに改良し、全種プロテアーゼ阻害剤について、短時間で変異株に関して、全ての検体について十分に信頼性の高い予測ができるようにする必要がある。

F. 研究発表

1. 論文発表

- Ode, H., Ota, M., Neya, S., Hata, M., Sugiura, W., Hoshino T., "Resistant Mechanism against Nelfinavir of Human Immunodeficiency Virus Type 1 Proteases", J. Phys. Chem. B 109, 564-574, 2005.

2. 学会発表

- Ode, H., Neya, S., Hata, M., Sugiura, W., Hoshino, T., "Insight into the Resistant Mechanism against HIV-1 Protease Inhibitor through Molecular Dynamics Simulations.", Int. Symp. on Molecular Nano-Engineering and Its Development into Microsystems, Tokyo, Japan, 60-61 (2004) Tokyo.

- Hattori, T., Yokoyama, M., Sato, H., Hoshino, T., "Computational Identification of HIV-1 Specific CTL Epitopes", Int. Symp. on Molecular Nano-Engineering and Its Development into Microsystems, Tokyo, Japan, 60-61 (2004) Tokyo.

- Fuji, H., Yokomaku, Y., Syouji, Y., Narita, T., Miyauchi, K., Matsuda, Z., Sato, H., Hoshino, H., Hoshino, T., "Construction of HIV-1 *env* Clone Library -Rapid Cloning and Expression of HIV-1 *env*, and Production of Recombinant HIV-1", Int. Symp. on Molecular Nano-Engineering and Its Development into Microsystems, Tokyo, Japan, 60-61 (2004) Tokyo.

- 太田雅美、簾貴士、大出裕高、畑晶之、佐藤武幸、横幕能行、布施晃、杉浦亙、星野忠次 「臨床応用に向けたコンピュータによるエイズ治療薬の適正予測」第 18 回日本エイズ学会学術集会・総会抄録集, 234 (2004) 静岡

- 藤秀義、田中真理、宮内浩典、松田善衛、星野忠次、有吉紅也、星野洪郎、佐藤裕徳、横幕能行 「HIV-1*env* クローンライブラリー作成の試みーHIV-1*env* の迅速なクローニング、発現および組み換えウイルス作成システム構築ー」第 18 回日本エイズ学会学術集会・総会抄録集, 311 (2004) 静岡

- 星野忠次, 太田雅美, 簾貴士, 大出裕高, 畑晶之, 根矢三郎, 横幕能行, 佐藤武幸, 杉浦亙, 布施晃 「計算機によるエイズウィルスの薬剤耐性評価」 第 48 回日本薬学会関東支部大会講演要旨集, 20 (2004) 千葉

- 大出裕高, 根矢三郎, 畑晶之, 杉浦亙, 星野忠次 「HIV-1 プロテアーゼのアミノ酸変異による阻害剤耐性機構の解明」 第 48 回日本薬学会関東支部大会講演要旨集, 45 (2004) 千葉

- 藤秀義, 横幕能行, 庄司祐介, 成田友之, 宮内浩典, 松田善衛, 佐藤裕徳, 星野洪郎, 根矢三郎, 星野忠次 「HIV*env* の迅速クローニング・

発現・組み換えウイルス作製システムの構築と基礎・臨床応用」 第48回日本薬学会関東支部大会講演要旨集, 96 (2004) 千葉

- 大出裕高, 畑晶之, 根矢三郎, 杉浦亙, 星野忠次 「分子動力学法を用いた HIV-1 Protease 阻害剤耐性機構の解明」情報計算化学生物学会2004年大会予稿集, 75-76 (2004) 東京
- 藤秀義, 庄司祐介, 宮内浩典, 星野忠次, 根矢三郎, 松田善衛, 横幕能行 「Non-Clade B を含む HIV-1 感染者由来 env 発現系の構築」 レトロウィルス研究会夏期セミナー (2004) 千葉
- 庄司祐介, 大出裕高, 藤秀義, 横幕能行, 根矢三郎, 星野忠次 「コンピューターシミュレーションでタンパク質構造予測はどこまで可能か？」 レトロウィルス研究会夏期セミナー (2004) 千葉
- 大出裕高, 太田雅美, 畑晶之, 根矢三郎, 杉浦亙, 星野忠次 「HIV-1protease 阻害剤耐性の分子動力学的評価」 日本薬学会第124年会要旨集－3, 29 (2004) 大阪

G. 知的所有権の出願・取得状況（予定を含む）
　　実績無し。

雑誌

発表者氏名	論文タイトル名	発表雑誌名	巻号	ページ	出版年
Ode H, Ota M, Neya S, Hata M, Sugiura W, Hoshino T	Resistant Mechanism against Nelfinavir of Human Immunodeficiency Virus Type 1 Proteases.	Journal of Physical Chemistry B	Vol.109, No.1	565-574	2005
Shiomi K, Matsui R, Isozaki M, Chiba H, Sugai T, Yamaguchi Y, Masuma R, Tomoda H, Chiba T, Yan H, Kitamura Y, Sugiura W, Omura S, Tanaka H	Fungal phenalenones inhibit HIV-1 integrase.	Journal of Antibiotics	Vol. 58, No.1	65-68	2005
Zhu D, Taguchi N H, Goto M, Odawara T, Nakamura T, Yamada H, Kotaki H, Sugiura W, Iwamoto A, Kitamura Y	Influence of single-nucleotide polymorphisms in the multidrug resistance-1 gene on the cellular export of nelfinavir and its clinical implication for highly-active antiretroviral therapy.	Antiviral Therapy	Vol.9	929-935	2004
Sugiura W, Matsuda M, Chiba T, Kakizawa J, Nishizawa M, Miura H, Hamatake M, Ueda T, Fujino M, Yamamda K, Yamamoto N	Changes in Prevalence and Patterns of Drug Resistant Mutations in Japan-Summary of Nationwide HIV-1 Drug Resistance Surveillance Study (1996 to 2003) in Japan.	Antiviral Therapy	Vol. 9	S109	2004
Yan H, Chiba T, Kitamura Y, Nishizawa M, Fujino M, Yamamoto N, Sugiura W	Novel Small – Molecule Compounds which inhibit strand transfer activity of HIV-1 integrase.	Antiviral Therapy	Vol. 9	S6	2004
Yan H, Miyagi T, Satoh E, Sugiura W,	Phenotype and function of GM-CSF independent dendritic cells generated by	Cellular Immunology	Vol.229, No.2	117-129	2004

Yamamoto N, Kimura H	long-term propagation of rat bone marrow cells.				
Saeng A.S, Wichukchinda N, Myint L, Pathipvanich P, Ariyoshi K, Rojanawiwat A, Matsuda M, Sawanpanyalert P, Sugiura W, Auwanit W	Study of Antiretroviral Drug Resistant HIV-1 Genotypes in Northern Thailand : Role of Mutagenically Separated Polymerase Chain Reaction as a Tool for Monitoring Zidovudine — Resistant HIV-1 in Resource — Limited Settings.	Journal of Acquired Immune Deficiency Syndromes	Vol.36, No.5	1051-1056	2004
Myint L, Matsuda M, Matsuda Z, Yokomaku Y, Chiba T, Okano A, Yamada K, Sugiura W	Gag Non-Cleavage Site Mutations Contribute to Full Recovery of Viral Fitness in Protease Inhibitor-Resistant Human Immunodeficiency Virus Type-1.	Antimicrobaial Agents and Chemotherapy	Vol.48, No.2	444-452	2004
Ariyoshi K, Matsuda M, Miura H, Tateishi S, Yamada K, Sugiura W	Patterns of Point Mutations Associated With Antiretroviral Drug Treatment Failure in CRF01_AE (Subtype E) Infection Differ From Subtype B Infection	Journal of Acquired Immune Deficiency Syndromes	Vol.33,	336-342	2003
Myint L, Matsuda M, Chiba T, Yan H, Kakizawa J, Okano A, Hamatake M, Nishizawa M, Sugiura W	Analysis of virion morphology and assembly process in protease inhibitor-resistant HIV-1	Antiviral Therapy	Vol.8	S91	2003
Sugiura W, Shimada K, Matsuda M, Chiba T, Myint L, Okano A, Yamada K	Novel Enzyme Linked Minisequence Assay for Genotypic Analysis of Human Immunodeficiency Virus Type 1 Drug Resistance.	Journal of Clinical Microbiology	Vol.41, No.11	4971-4979	2003
杉浦 亙	HIV の薬剤耐性研究の現状と今後の課題	現代医療	Vol.35, No.6	113-118	2003
杉浦 亙	日本における薬剤耐性HIV-1の現状	臨床とウィルス	Vol.31, No.4	272-282	2003

565

Resistant Mechanism against Nelfinavir of Human Immunodeficiency Virus Type 1 Proteases

Hirotaka Ode,* **Masami Ota, Saburo Neya, Masayuki Hata, Wataru Sugiura,†** and **Tyuji Hoshino**

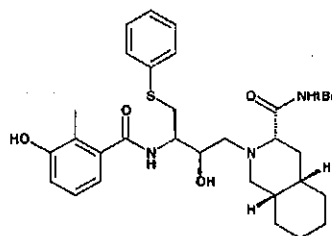*Graduate School of Pharmaceutical Sciences, Chiba University, Chiba 263-8522, Japan*

Received: July 15, 2004; In Final Form: October 12, 2004

Inhibitors against human immunodeficiency virus type-1 (HIV-1) proteases are finely effective for anti-HIV-1 treatments. However, the therapeutic efficacy is reduced by the rapid emergence of inhibitor-resistant variants of the protease. Among patients who failed in the inhibitor nelfinavir (NFV) treatment, D30N, N88D, and L90M mutations of HIV-1 protease are often observed. Despite the serious clinical problem, it is not clear how these mutations, especially nonactive site mutations N88D and L90M, affect the affinity of NFV or why they cause the resistance to NFV. In this study, we executed molecular dynamics simulations of the NFV-bound proteases in the wild-type and D30N, N88D, D30N/N88D, and L90M mutants. Our simulations clarified the conformational change at the active site of the protease and the change of the affinity with NFV for all of these mutations, even though the 88th and 90th residues are not located in the NFV-bound cavity and not able to directly interact with NFV. D30N mutation causes the disappearance of the hydrogen bond between the *m*-phenol group of NFV and the 30th residue. N88D mutation alters the active site conformation slightly and induces a favorable hydrophobic contact. L90M mutation dramatically changes the conformation at the flap region and leads to an unfavorable distortion of the binding pocket of the protease, although 90M is largely far apart from the flap region. Furthermore, the changes of binding energies of the mutants from the wild-type protease are shown to be correlated with the mutant resistivity previously reported by the phenotypic experiments.

Introduction

Replication of human immunodeficiency virus type 1 (HIV-1) requires the processing of gag and gag-pol polyprotein precursors by the virus-encoded aspartic protease, so-called HIV-1 protease.[1] Therefore, the protease has been one of the major targets of anti-HIV-1 treatments.[2] Today, seven protease inhibitors (PIs) are approved by the FDA and are available clinically. Those drugs are well-designed to fit the inside of the binding cavity, mimicking the configuration of a substrate in the transition state for the hydrolysis reaction by the protease.[3] However, HIV-1 frequently acquires the resistance to these inhibitors through specific mutations due to the high polymorphism and adaptability of the protease.[4–7] Serious resistant mutants survive during the treatment with PIs and cause a failure in long-term HIV chemotherapy.

Among patients who failed in the treatment with nelfinavir, NFV (Figure 1), which is one of the PIs, substitutions of asparagine (N) for aspartic acid (D) at codon 30 (D30N), aspartic acid for asparagine at codon 88 (N88D), and methionine (M) for leucine (L) at codon 90 (L90M) are frequently seen in HIV-1 protease.[8,9] D30N is a primary NFV-resistant mutation, which appears to be very specific for this inhibitor. N88D is an additional mutation to D30N. A combination of D30N and N88D is the most commonly seen in patients treated with NFV, and N88D compensates for the loss of replicative capacity resulting from D30N as a secondary mutation. L90M is a primary mutation responsible for the resistance to both NFV
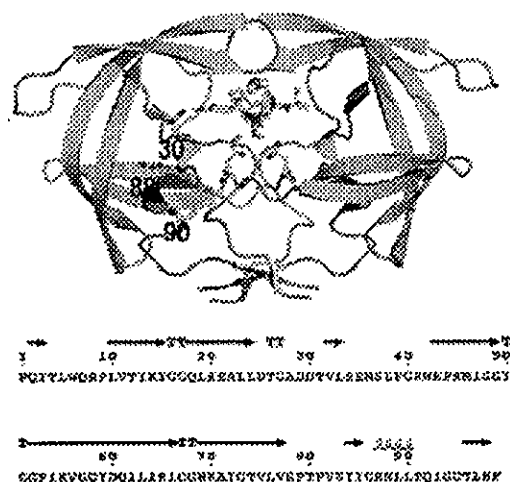
* Corresponding author. Tel.: +81-43-290-2926. Fax: +81-43-290-2925. E-mail: odehir@graduate.chiba-u.jp.
† AIDS Research Center, National Institute of Infectious Diseases, Musashimurayama, Tokyo 208-0011, Japan.

Figure 1. Structure of NFV. According to the crystal structure (PDB code: 1OHR), the *m*-phenol group of the 2-methyl-3-hydroxylbenzamide side chain of NFV interacts with 30D by hydrogen bonding in the S2 pocket of HIV-1 protease. The *tert*-butylcarboxamide moiety occupies the S2′ subsite, the S-phenyl group and dodecahydroisoquinoline ring fit into the hydrophobic S1 and S1′ pockets, and the central hydroxyl group is bound to the catalytic aspartates.

and saquinavir[10] and also appears to be associated with the resistance to the other PIs.[4–6] There are two evolutionarily possible pass ways for the NFV-related mutation acquisition, and the L90M acquisition pass way is evolutionarily different from the pass way of D30N.[11,12]

The three-dimensional X-ray structure of the NFV-bound protease[13] implies that D30N mutation would alter the direct electrostatic interaction with the *m*-phenol group of NFV at the active site (Figure 2). It is, however, difficult to understand the NFV resistance due to N88D or L90M mutations because these 88th and 90th residues are located at the nonactive site near the dimer interface. Recently, Mahalingam and co-workers determined some high-resolution X-ray crystal structures of D30N, N88D, or L90M mutants combined with peptide inhibitor analogues, not NFV,[14–16] and suggested the mechanism of the resistance. They found that D30N mutation altered the interac-

566 *J. Phys. Chem. B, Vol. 109, No. 1, 2005*

Ode et al.

Figure 2. X-ray structure of the HIV-1 protease/NFV complex (PDB code: 1OHR). Locations of the two catalytic aspartates and the residues related with NFV resistance (30, 88, 90) are shown in the stick representation in one subunit of the protease dimer. The wild-type sequence is shown below.

tion with the inhibitors, N88D mutation lost the water that mediated hydrogen bond interactions among 31T, 74T, and 88D, and L90M caused an unfavorable van der Waals contact between 24T/25D and the long side chain of 90M. Further, they reported that L90M mutants altered the active site conformation when indinavir entered the binding cavity of the protease.[17] Though these structural features might be seen in the proteases complexed with NFV, a clear explanation on the resistance to NFV due to these mutations has not been provided yet.

Computational chemistry has been developed in recent years, and detailed analysis has been significantly improved. Many computational works were already carried out to clarify the catalytic mechanism of HIV-1 protease in its substrate-hydrolysis reaction.[18–30] And the other works discussed the drug-resistant mechanisms of some familiar active site mutations.[31–36] In the present study, we discussed the resistant mechanism of not only active site mutation D30N but also nonactive site mutations N88D, L90M. To clarify these mechanisms, we investigated the wild-type HIV-1 protease and D30N, N88D, D30N/N88D, and L90M mutants complexed with NFV on the basis of the molecular dynamics (MD) approach explicitly including the solvate condition. Our MD simulations for each mutant demonstrated the respective resistant mechanisms to NFV. Not only active site mutation D30N but also nonactive site mutations N88D and L90M affect the interaction between NFV and the protease through the structural modification of the binding cavity. There are no papers reported on the resistant mechanism of the nonactive site mutations through a computational approach. The atom-level understanding of the origins of these resistances will be useful in the design of better PIs. Further, our work suggests the possibility to reproduce the experimental phenotype data from the results of MD simulation.

Materials and Methods

MD Simulation. The reliability of MD simulations largely depends on the selection of force field parameters and the assignment of atomic charges. Hence, the electrostatic potential of NFV was preliminarily calculated at the B3LYP/6-31G(d, p) level using the Gaussian 98 program[37] after geometry optimization. The partial atom charges for NFV utilized in the MD simulation were determined using the RESP method[38] so

that the atom charges could reproduce the values of the calculated electrostatic potential at the surrounding points of NFV. The charges were set equal between two atoms if they are the same element and have the same bond coordination. Afterward, all the minimizations and MD simulations were executed with the Sander module of AMBER 7 package.[39] The AMBER parm99 force field[40] was used as the parameters for the van der Waals and the bonded energy terms.

Each initial structure for the wild-type protease of clade B and D30N, N88D, D30N/N88D, and L90M mutants complexed with NFV was modeled on the basis of the coordinates of an X-ray crystal structure (PDB code: 1OHR)[13] using the LEaP module. All the crystal waters were included in each model. Each model was placed in a periodic cubic box filled with the about 8000 TIP3P water molecules.[41] The cutoff distance for the long-range electrostatic and the van der Waals terms was 12.0 Å. All covalent bonds to hydrogen atoms were constrained using the SHAKE algorithm.[42] Periodic boundary conditions were applied to avoid the edge effects in all calculations. Energy minimization was achieved via three stages. At first, the movement was allowed only for the water molecules. Next, the ligand and the mutated residues were allowed to move in addition to the water molecules. Last, all atoms were permitted to move freely. In each stage, energy minimization was executed by the steepest decent method for the first 1000 steps and the conjugated gradient method for the subsequent 3000 steps. The protonation states of the catalytic aspartates 25D/25'D were determined performing energy minimizations for all combinations of the protonation states (25D/25'D both protonated, 25D/25'D both unprotonated, 25D protonated and 25'D unprotonated, 25D unprotonated and 25'D protonated). The combination with protonated 25D and unprotonated 25'D showed the lowest total potential energy. This protonation state is consistent with the results of the previous work by Zoete et al.[43]

After 24-ps heating calculations until 300 K using the NVT ensemble, MD simulations were executed using the NPT ensemble at 1 atm and at 300 K for more than 1 ns, with a basic time step of 1 fs. After 500-ps equilibrating calculations, the MD simulations showed no large fluctuations (the deviation of the root-mean square deviation, RMSD, of the main chain is less than 0.1 Å in each model; more detailed data are shown in Supporting Information). Coordinates of 200 snapshots at the intervals of 0.5 ps were obtained as structural data; those were collected for the last 100 ps of the simulations.

Difference Distance Plot. The difference distance plots are drawn to assess the intermolecular relative shifts in response to the mutation. First, $C\alpha_i$-to-$C\alpha_j$ distances, d_{ij}^A, are computed for all the combinations of the $C\alpha$ atoms in the protease of a mutant (A). Second, the same distances, d_{ij}^B, are measured for the wild-type model (B). The difference distances d_{ij}^{AB} of the residues i and j are given by
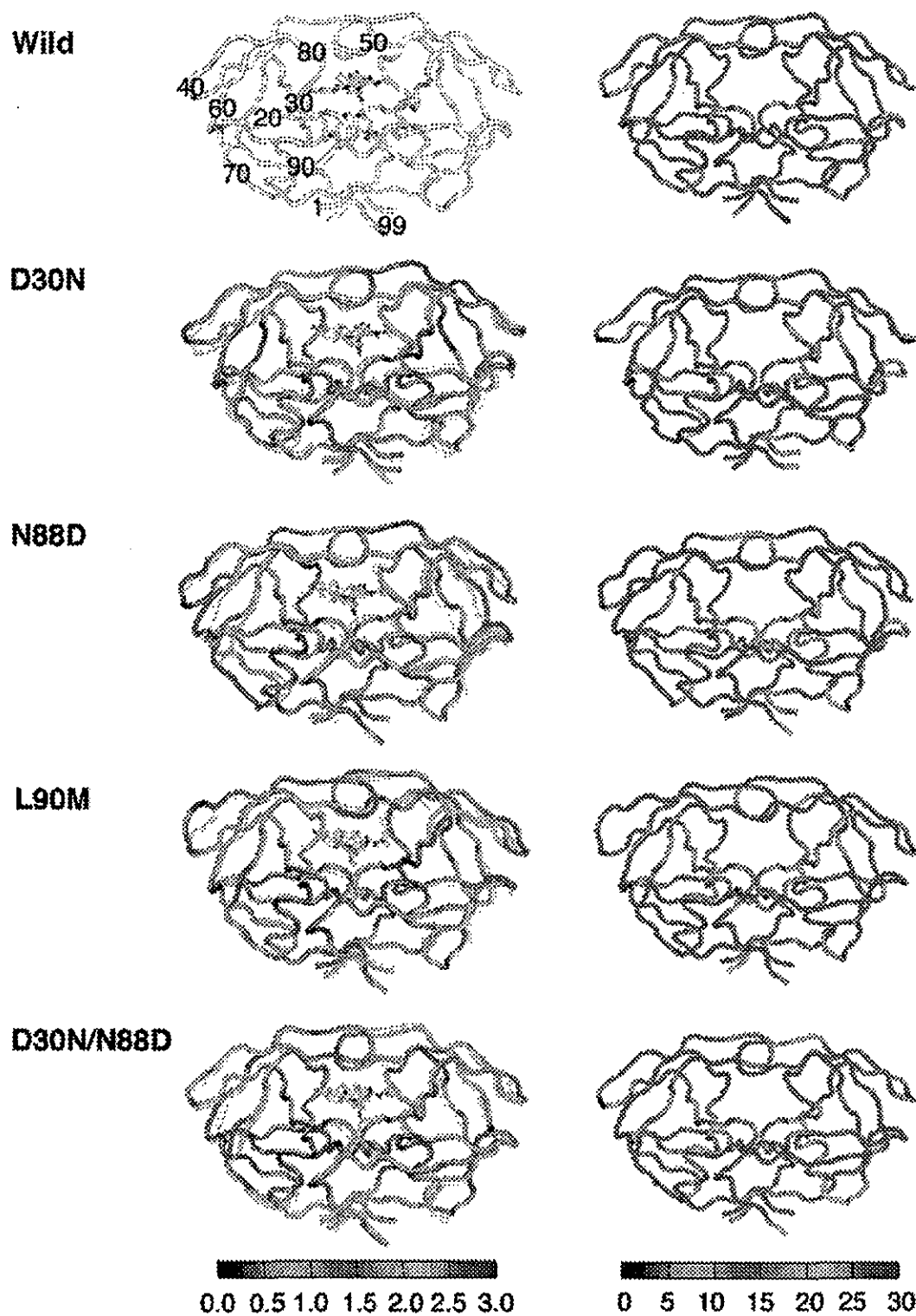
$$D_{ij}^{AB} = |d_{ij}^A - d_{ij}^B|$$

Further, the error-scaled difference distance[44,45] E_{ij}^{AB} is estimated by

$$E_{ij}^{AB} = D_{ij}^{AB}/\sigma(D_{ij}^{AB})$$

$$\sigma(D_{ij}^{AB}) = [(\sigma_{r,i}^A)^2 + (\sigma_{r,j}^A)^2 + (\sigma_{r,i}^B)^2 + (\sigma_{r,j}^B)^2]^{1/2}$$

where $\sigma_{r,i}^A$ is the radial positional error that corresponds to the uncertainty for an individual atom position. The difference distance is plotted on the lower left panel, and the error-scaled

Figure 3. Left: Plots of RMSD between the average structures of the wild-type protease and each mutant, traced over every main chain atom. Each mutant structure is superimposed on the wild-type structure represented by white tubes. Right: B-factor values for main chain atoms in the wild-type and mutated proteases. The color represents the magnitude of the RMSD and B-factor shown at the lower bar. Scales are in units of angstroms and squared angstroms, respectively.

difference distance is on the upper right one in the two-dimensional map of Figure 4 as a function of residue numbers by using GNUPLOT.[46]

Hydrogen Bond Criterion. The formation of a hydrogen bond was defined in terms of distance and orientation. The combination of donor D, hydrogen H, and acceptor A atoms

D30N

N88D

L90M

D30N/N88D
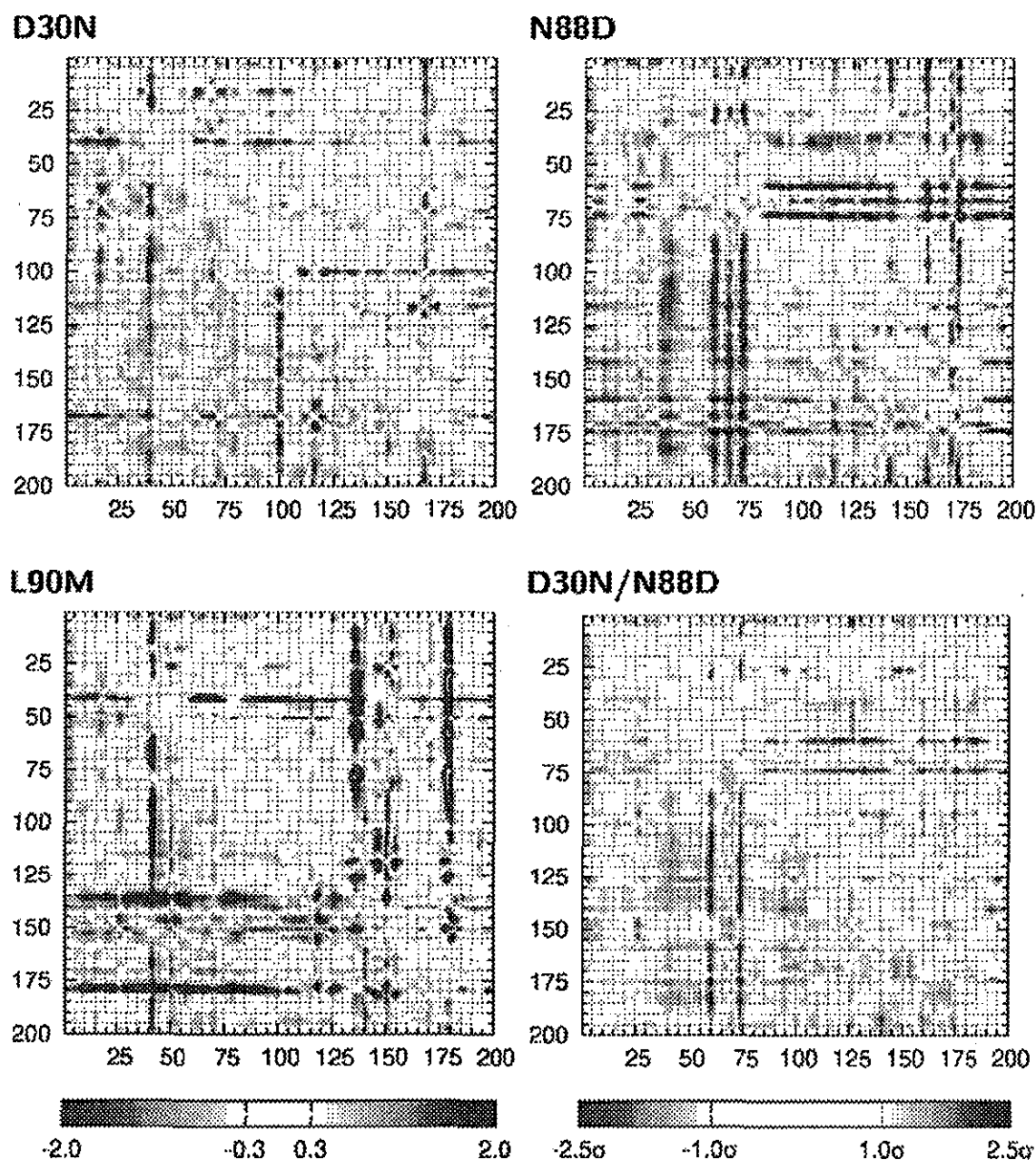
Figure 4. Difference distance matrixes and error-scaled difference matrixes for the Cα atoms. The difference distances for all pairs of residues in the protease are shown on the lower panel. The color represents the magnitude, as shown on the bar on the lower left. The upper right panel shows the error-scaled difference distance matrixes. Changes greater than 1.0σ and smaller than 2.5σ are colored as seen on the lower right bar. Numbers 1−99 represent the residues from 1P to 99F, and numbers 101−199 represents the residues from 1′P to 99′F.

with a D−H···A configuration is regarded as a hydrogen bond when the distance between donor D and acceptor A is shorter than R_{max} and the angle H−D−A is smaller than Θ_{max}. The values of 3.5 Å and 60.0° were adopted for R_{max} and Θ_{max} in this study.

Buried Surface Area (SA). The solvate accessible SA[47] was computed with Paul Beroza's molsurf program, which was based on the analytical technique primarily developed by Connolly[48] to evaluate the surface area buried by a ligand in binding to the enzyme. The SA is computed for the NFV-bound protease structure. SA is also calculated both for only NFV and for the free protease. The difference in SA values between the bound

and the unbound cases is defined as the SA buried on complexation.[49]

Binding Energy Calculation. The binding free energy[50] is calculated on the basis of the next equation:

$$\Delta G_b = \Delta G_{MM} + \Delta G_{sol} - T\Delta S$$

where ΔG_b is the binding free energy in solution, ΔG_{MM} is the interaction energy between the ligand and the protein, ΔG_{sol} is the solvation energy, and $-T\Delta S$ is the conformational entropy contribution to the binding. When it is assumed that the entropies are almost the same in magnitude among the mutants, the

difference in entropy is disregarded in the comparison of the binding energy in this study. ΔG_{MM} is calculated from molecular mechanics (MM) interaction energy:

$$\Delta G_{MM} = \Delta G_{int}^{ele} + \Delta G_{int}^{vdw}$$

where ΔG_{int}^{ele} and ΔG_{int}^{vdw} are electrostatic and van der Waals interaction energies between a ligand and a protein. These energies are computed using the same parameter set with the simulation, and no cutoff is applied for the calculation. Solvation energy ΔG_{sol} can be divided into to the two parts:

$$\Delta G_{sol} = \Delta G_{sol}^{ele} + \Delta G_{sol}^{nonpol}$$

The electrostatic contribution to the solvation free energy (ΔG_{sol}^{ele}) is calculated with the Poisson–Boltzmann method using DelPhi program.[51] The hydrophobic contribution to the solvation free energy (ΔG_{sol}^{nonpol}) is determined as a function of the solvent-accessible surface area.[52]

Results

Conformational Changes of the Protease. To study the mechanism of the drug resistance, we compared the averaged atom coordinates of the wild-type with those of each mutant. The least-squared rigid body superposition indicates that no large conformational alteration appears in the shape of the protease for every mutant, as shown in the left column of Figure 3. The RMSD measurement was executed by using the coordinates of backbone atoms N, Cα, and C in the superimposed structures of the wild-type and each mutant. The RMSD values compared with the wild-type model is 0.8 Å in the D30N, 0.9 Å in the N88D, 1.1 Å in the L90M, and 0.6 Å in the D30N/N88D mutant model, averaged over the whole structure. The detailed analysis of individual residues and the comparison of the local structures, however, provided new understanding on the conformational changes due to the mutation. Although large deviations are seen at the residues of the outside loop region, those residues are not minutely examined because their large fluctuations are commonly observed irrelevant to the mutations in B-factor analysis.[43,53] The most characteristic conformational change is detected in the L90M mutant structure. The L90M mutant structure of our study displays significant backbone deviations at the flap regions (43K-58Q, 43′K-58′Q) and at the 79′P loop (78′G-84′I). The RMSD values are 1.6 Å at the flap of one subunit, 2.0 Å at the opposite flap, and 1.9 Å at the 79′P loop. Those values are very large compared with those of the other mutants (0.5 Å/0.6 Å/0.7 Å in D30N, 0.6 Å/0.7 Å/0.7 Å in N88D, and 0.5 Å/0.6 Å/0.5 Å in D30N/N88D). It should be emphasized that, though the 90th residue is not located at the flap nor at the 79′P loop, L90M affects the conformation at those regions. In the N88D mutant structure, peculiar conformational changes occur at the β sheets consisting of 59Y-75V (RMSD: 1.4 Å) and 59′Y-75′V (RMSD: 1.2 Å). Those regions move far away from the helix region (87R-90L/87′R-90′L). The D30N/N88D mutant structure exhibits the similar conformational changes at the same but much narrower regions of those β sheets: 74T/74′T and its vicinity.

To interpret small and more detailed conformational differences, we compared pairwise Cα–Cα distances in the averaged coordinates of each mutant model with those of the wild-type. Each difference distance is shown in the lower left panel of the map in Figure 4, and the upper right panel shows the error-scaled difference distance.[44,45] Figure 4 also indicates that the L90M model has large conformational changes at the flap region

(50I/50′I and its vicinity) and at the loop region at 79′P. The N88D and D30N/N88D models alter the conformations at the β sheets (74′T and its vicinity). In addition, these maps provide more detailed comprehension. The flap conformational alteration in the L90M mutant is owing to the approach of 50I to the triads (25D26T27G/25′D26′T27′G) and the detachment of 50′I from the triads. 79′P, 81′P, and some residues at the same loop are far apart from the residues at the opposite subunit. This loop moves outward and also creates a distance from NFV. The mutants other than L90M exhibit the common structural alteration. For example, the distance between the triad and the flap region is slightly changed. The RMSD from the wild-type at the triads in each subunit is 0.8 Å/1.0 Å (D30N), 0.8 Å/1.2 Å (N88D), and 0.8 Å/1.1 Å (D30N/N88D). These deviations are much larger, compared to the RMSD at the flap region. Hence, characteristic distortion in D30N, N88D, and D30N/N88D is mainly caused by the conformational change of the triad.

The above conformational changes were seen in the last 100 ps of simulation. To ensure that these changes were not just from the local fluctuations of MD simulations, we examined the coordinates for the last 500 ps of simulation. The analysis of the last 500 ps of simulation brought us similar results about the conformational changes. L90M had large deviations at the flap (RMSD: 1.5 Å/1.8 Å) and at the 79′P loop (1.7 Å), compared with wild-type structure. The N88D mutation induced the conformational change at the β sheets around 74T/74′T. In N88D, the RMSD values of the β sheets are 1.4 and 1.2 Å in each subunit. And in D30N/N88D, they are both 0.9 Å. Furthermore, the RMSD values at the triads are 0.8 Å/1.1 Å in D30N, 0.7 Å/1.1 Å in N88D, and 0.8 Å/1.1 Å in D30N/N88D.

Hydrophilic Interactions between NFV and the Protease. In protease–ligand interactions, hydrogen bonds play a crucial role in stabilizing the complex. Hydrogen bonds between the protease and NFV in every model are listed in Table 1. Analysis of the protease–NFV hydrogen bonds suggests that mutation has obviously affected the protease–NFV hydrogen bond network. Only a few residues are responsible for the hydrogen bonds with NFV. Hydrogen bond networks consist of 25D/25′D (catalytic aspartates), 50I/50′I, 30D, 29′D, some water molecules, and NFV. The direct interaction between the carboxyl group of 25′D and the central hydroxyl group of NFV is very frequently seen in every model, whereas the protonated aspartate 25D hardly interacts with NFV, except for the L90M model. At the S2 pocket, the main chain of 30D interacts with the *m*-phenol group of NFV. In the wild-type, the main chain of 30D directly interacts with NFV. In each of the N88D and L90M models, one water molecule links 30D and NFV with a hydrogen bond chain although the distance between the donor and the acceptor atoms is elongated. On the other hand, no hydrogen bond is observed in the mutated D30N and D30N/N88D models. D30N mutation causes the disappearance of the hydrogen bond network at the S2 pocket, because those mutants increase the distances with the *m*-phenol group of NFV and cannot keep any water molecule. At the flap region, one water molecule exists in the neighbor of 50I and/or 50′I and NFV in all models. This water intermediates the intramolecular and intermolecular hydrogen bonds, which results in stabilizing the protease–NFV complex. In the wild-type model, the water links the main chain of 50′I with NFV. Further, a direct hydrogen bond between the sulfur atom of NFV and the main chain of 50I is detected and no water molecule mediates the hydrogen bond from 50I. In contrast, the water mediates the hydrogen bond between NFV and both 50I and 50′I in the D30N model. NFV forms a hydrogen bond network with either 50I or 50′I in the other

TABLE 1: Hydrogen Bond Network in Each Model[a]

		donor			acceptor		occupancy (%)
wild	catalytic domain	O21	−HOL	(NFV)	OD1	(25′D)	91.0
		O21	−HOL	(NFV)	OD2	(25′D)	95.5
		O	−H2	(WAT208)	O21	(NFV)	60.0
		O	−H1	(WAT208)	OD2	(25′D)	61.0
		N22	−HNM	(NFV)	O	(WAT208)	59.5
	S2 pocket	O38	−HO	(NFV)	O	(30D)	90.0
		N	−H	(30D)	O38	(NFV)	64.5
	flap region	N	−H	(50I)	S74	(NFV)	61.0
		O	−H1	(WAT205)	O17	(NFV)	51.5
		N	−H	(50′I)	O	(WAT205)	61.0
D30N	catalytic domain	O21	−HOL	(NFV)	OD2	(25′D)	100.0
		N22	−HNM	(NFV)	O	(WAT210)	85.0
		O	−H1	(WAT210)	O21	(NFV)	52.5
	flap region	O	−H2	(WAT207)	O17	(NFV)	76.5
		O	−H1	(WAT207)	O25	(NFV)	89.0
		N	−H	(50I)	O	(WAT207)	50.5
		N	−H	(50′I)	O	(WAT207)	93.5
	S2′ pocket	N12	−HNC	(NFV)	O	(WAT4757)	94.5
		N	−H	(29′D)	O	(WAT4757)	85.0
		O	−H2	(WAT4757)	OD1	(29′D)	52.5
N88D	catalytic domain	O21	−HOL	(NFV)	OD2	(25′D)	100.0
	S2 pocket	O	−H1	(WAT3880)	O38	(NFV)	59.0
		N	−H	(30D)	O	(WAT3880)	87.5
		O	−H2	(WAT3880)	O	(30D)	97.5
	flap region	O	−H2	(WAT203)	O17	(NFV)	79.5
		O	−H1	(WAT203)	O25	(NFV)	95.0
		N	−H	(50′I)	O	(WAT203)	100.0
D30N/N88D	catalytic domain	O21	−HOL	(NFV)	OD2	(25′D)	96.5
	flap region	O	−H2	(WAT205)	O25	(NFV)	98.5
		O	−H1	(WAT205)	O17	(NFV)	97.5
		N	−H	(50′I)	O	(WAT205)	96.5
L90M	catalytic domain	O21	−HOL	(NFV)	OD2	(25′D)	100.0
		OD2	−HD2	(25D)	O21	(NFV)	90.5
	S2 pocket	O	−H1	(WAT3836)	O38	(NFV)	73.5
		N	−H	(30D)	O	(WAT3836)	90.0
		O	−H2	(WAT3836)	O	(30D)	99.5
	flap region	O	−H2	(WAT205)	O17	(NFV)	96.5
		O	−H1	(WAT205)	O25	(NFV)	97.5
		N	−H	(50I)	O	(WAT205)	90.5
	S2′ pocket	N12	−HNC	(NFV)	O	(WAT4349)	93.5
		N	−H	(29′D)	O	(WAT4349)	74.5
		O	−H2	(WAT4349)	OD1	(29′D)	74.5

[a] The listed donor and acceptor pairs satisfy the criteria for the hydrogen bond over 50.0% of the time during the last 100 ps of simulation. The nomenclature of the atoms is the same as that of 1OHR.

models (L90M, N88D, and D30N/N88D). Both NFV and the water molecule hardly interact with main chain of 50'I in the L90M mutant and with the main chain of 50I in the N88D and D30N/N88D mutants. Hence, each of the N88D and L90M mutations weakens the hydrogen bond networks around 50I and 50'I, respectively. Interestingly, a water molecule mediating a hydrogen bond with 29'D in the S2 pocket is frequently observed in the simulations of D30N and L90M mutants. Another water molecule mediating an intramolecular hydrogen bond in NFV is located near the catalytic aspartates in both the wild-type and the D30N models (WAT208 and WAT207, respectively). In the wild-type model, this water simultaneously mediates the hydrogen bond between 25'D and NFV.

In addition to the NFV—protease interaction at the active site, the N88D mutation modulates the hydrogen bond network at the surroundings of the 88th residues (Figure 5). In the wild-type, the main chain of 88N has a direct hydrogen bond with the main chain of 29D, and the side chain of 88N interacts with the side chain of 31T. Those hydrogen bonds are also observed in the opposite subunit. Further, one water molecule links 88N with 74T (occupancy is 93.5%) and 88'N with 74'T (75.5%). In each of the D30N and L90M, the 88th residues in both
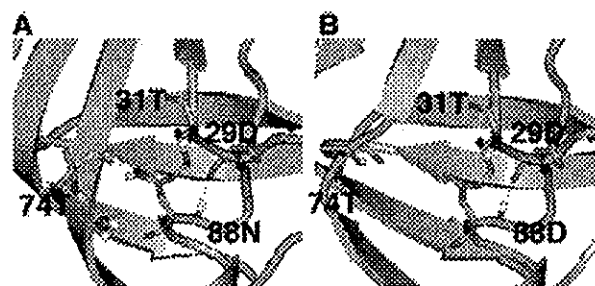
Figure 5. Hydrogen bond network surrounding the 88th residue. A: Wild-type protease structure. B: N88D mutant protease structure.

subunits also have the same hydrogen bond networks as the 29th, 31st, and 74th residues. But in the N88D and D30N/N88D mutant, the water-mediated hydrogen bond does not exist. That is, the N88D mutation induces the disappearance of the hydrogen bonds mediated by water molecules, though the direct hydrogen bonds are retained.

Hydrophobic Interactions between NFV and the Protease. Hydrophobic interactions and van der Waals interactions also contribute to stabilizing the complex. We evaluated the SA

Resistant Mechanism against NFV of HIV-1 PR

J. Phys. Chem. B, Vol. 109, No. 1, 2005 **571**

TABLE 2: Buried SA and the Contribution of Hydrophobic and Hydrophilic Residues

	buried SA (Å²)	hydrophobic/hydrophilic[a]
wild	805.9	83.0:17.0
D30N	809.9	82.8:17.2
N88D	841.5	83.1:16.9
D30N/N88D	832.6	86.1:13.9
L90M	765.2	87.1:12.9

[a] Hydrophobic residue: Gly/Ala/Val/Leu/Ile/Met/Pro/Phe/Trp. Hydrophilic residue: Ser/Thr/Asn/Gln/Tyr/Cys/Lys/Arg/His/Asp/Glu.
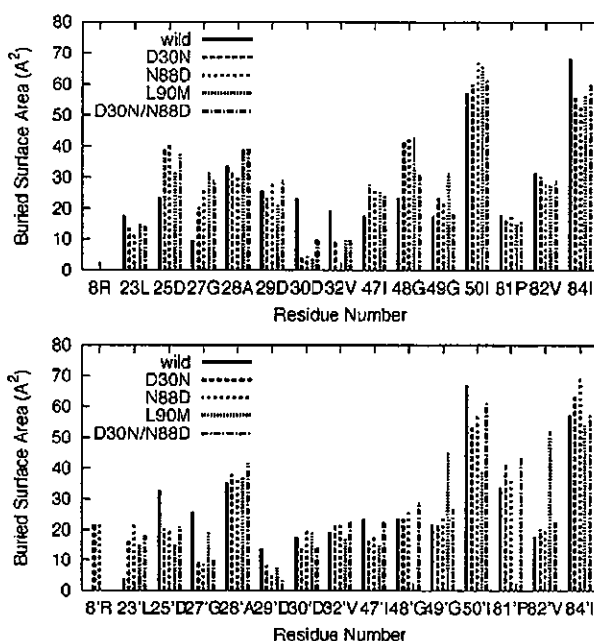
Figure 6. Buried SAs due to each involved residue. The upper graph represents those of one subunit, and the lower graph represents those of the other subunit. L90M shows notable differences at 48'G, 81'P, and 82'V from the other mutants.

buried by the complexation, which is related with the hydrophobicity of the binding cavity and the magnitude of van der Waals contacts between the ligand and the enzyme.[54-56] The results in Table 2 and Figure 6 show that most of the buried residues are hydrophobic ones. The 2-methyl-3-hydroxylbenzamide moiety of NFV has hydrophobic contacts with 23L, 28A, and 84I of the protease at the S2 pocket, and the tert-butylcarboxamide moiety has contacts with 32'V and 47'I at the S2' pocket. Hydrophobic interactions are also seen between the dodecahydroisoquinoline ring and 23L, 28A, 81P, 82V, 84I, and 50'I of the protease at the S1 pocket and between the S-phenyl group and 50I, 23'L, 28'A, 81'P, 82'V, and 84'I at the S1' pocket. The stabilization caused by hydrophobic interaction is mainly due to 50I/50'I and 84I/84'I, and secondly 28A/28'A, 48G/48'G, and 81'P. The L90M mutant hardly has hydrophobic contacts with NFV at 48'G and 81'P. These little

hydrophobic contributions at 48'G and 81'P result in the serious decrease of the buried surface. The D30N mutation hardly affects the buried SA, whereas the N88D mutation increases the buried SA.

Binding Energy Calculation. Table 3 shows the binding energy between NFV and protease. Each mutation causes a distinctive energetic change from the wild-type. D30N decreases the electrostatic energy greatly. N88D becomes more stable because of the electrostatic contribution by the solvation effect than the wild-type. The D30N/N88D model has both characters of D30N and N88D models. D30N/N88D is less stable than N88D because of the electrostatic contribution and is more stable than D30N by the solvation effect. L90M causes a decrease of the electrostatic energy and a large decrease of the van der Waals energy. These energetic results are compatible with the indices of the resistance level that were estimated from experimental IC90.[8,9]

Discussion

We executed MD simulations to understand the resistance mechanism against NFV about not only active site mutation D30N but also N88D and L90M. The simulations suggest that these mutations affect the protease structures on complexation and the NFV—protease interactions, despite the location of the mutated residues.

D30N is a primary mutation of NFV, which emerges during the treatment with this inhibitor highly specifically. The X-ray crystal structure of the wild-type protease complexed with NFV[13] shows that the m-phenol group of NFV interacts with both main chain atoms and the side chain carboxyl group of 30D at the S2 pocket. Accordingly, the D30N mutation has been assumed to make less hydrophilic contacts and causes the disappearance of the hydrogen bond interaction from the 30th residue.

Clemente et al. investigated the D30N mutant protease using a docking study previously.[33] They concluded that the D30N mutant would maintain the hydrogen bond between 30N and NFV but weakens the strength of hydrogen bonding due to the decrease of acid—base interaction. However, their computational model could move only NFV and the side chain of 30N in the vacuum condition without any water molecules. That is, their docking simulations did not consider the contributions of the movement of the residues other than 30N nor water solvation effects. MD simulation is useful to incorporate these contributions and to provide more detailed information. The proton or water-mediated hydrogen bonds are observed between the m-phenol group of NFV and the main chain of 30D in the wild-type model and the other models having a sequence of 30D, although the side chain carboxyl oxygens of 30D have no hydrogen bonds with NFV. D30N cancels those hydrogen bonds and decreases the electrostatic interaction energy greatly. In addition, we find that the D30N mutation loses its ability to keep any water molecule at the S2 pocket. Then, the substitution of asparagine (N) for aspartate (D) at codon 30 is concluded to

TABLE 3: Binding Free Energies of the Wild-type and Mutants

	ΔG_{int}^{ele} (kcal/mol)	ΔG_{int}^{vdw} (kcal/mol)	ΔG_{sol}^{nonpol} (kcal/mol)	ΔG_{sol}^{ele} (kcal/mol)	$\Delta G_{int+sol}^{ele}$ (kcal/mol)	ΔG_b^{a} (kcal/mol)	resistance level[b]
wild	−26.5 ± 4.2	−66.4 ± 3.3	−4.5 ± 0.1	44.2 ± 3.4	17.7 ± 3.5	−53.2 ± 4.2	
D30N	−19.2 ± 2.8	−64.0 ± 2.8	−4.5 ± 0.2	38.2 ± 3.6	19.0 ± 3.7	−49.5 ± 3.5	6
N88D	−26.2 ± 3.5	−66.0 ± 3.5	−4.7 ± 0.3	42.6 ± 3.7	16.4 ± 3.6	−54.3 ± 3.9	0.6
D30N/N88D	−15.1 ± 3.9	−64.9 ± 3.3	−4.6 ± 0.2	35.4 ± 3.7	20.3 ± 3.8	−49.2 ± 4.0	6
L90M	−21.1 ± 3.5	−62.2 ± 3.0	−4.2 ± 0.2	36.4 ± 3.5	15.3 ± 4.0	−51.2 ± 4.0	5

[a] TΔS is not included. [b] References 8 and 9.
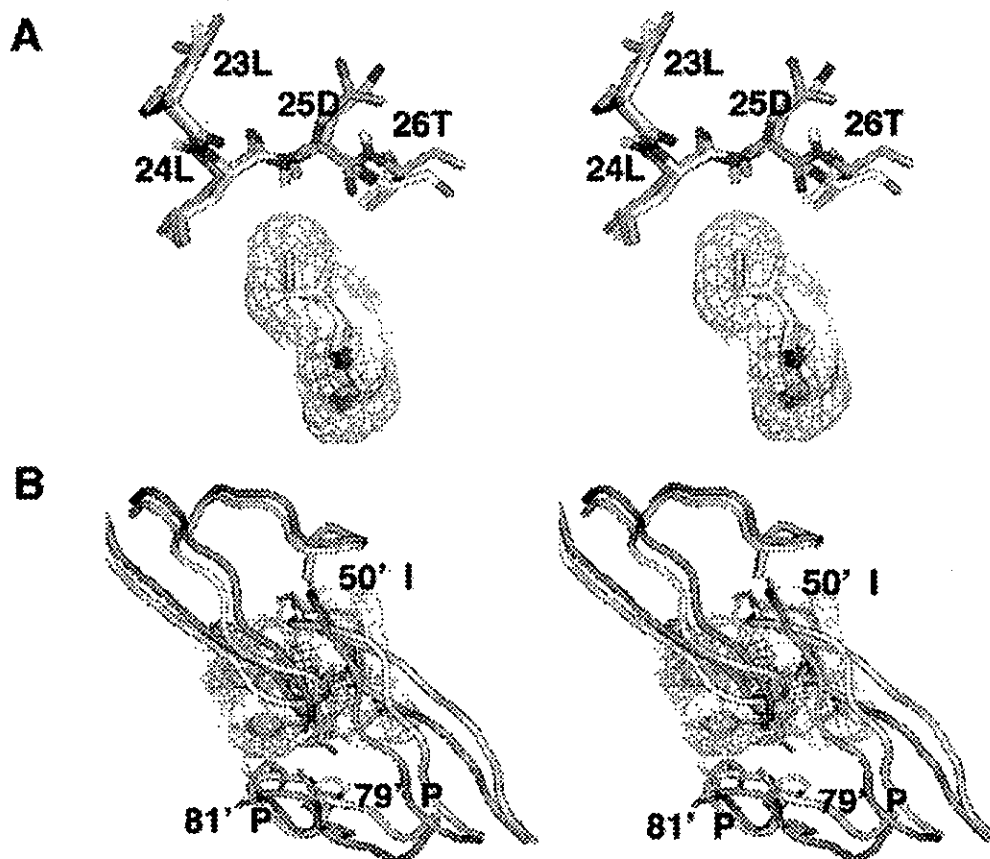
Figure 7. Stereoview of the structures (A) at the surrounding region of the 90th residue and (B) at the flap region. The wild-type structure is represented by white tubes, and L90M mutant is represented by blue tubes.

cause NFV resistance as a result of the serious decrease in the electrostatic interaction.

N88D is known as a secondary mutation for NFV and is frequently seen in the clinical scene next to D30N. Because the 88th residue is located at the helix region near the dimer interface, not at the active site, it is not clear why N88D substitution affects the resistance against NFV. Mahalingam and co-workers determined the X-ray crystal structure of the N88D mutant with substrate analogue inhibitors, not NFV.[14-16] They found that 88N in the wild-type had the proton and/or water-mediated interactions with 29D, 31T, and 74T in each subunit, whereas the corresponding water molecules were missing in both subunits of the N88D single mutant. It is also found from our calculation on the wild-type protease that the side chain of 88N makes a hydrogen bond network with 74T via one water molecule, the backbone nitrogen of 88N has a hydrogen bond with 29D, and the side chain oxygen of 88N interacts with 31T. These hydrogen bond networks are also observed in the opposite subunit. In contrast, in each of the N88D and D30N/N88D mutants, 88D interacts with only 31T and 29D, and the hydrogen bond mediating water molecules disappear in the respective subunit. That is, the 88th residue cannot form any hydrogen bonds with the 74th residue. This disappearance of the water-mediated hydrogen bond allows a large conformational change at the 74th residue. The conformational change at the β sheet consisting of the 74th residue and its adjacent contiguous residues induces the conformational changes at the neighboring β sheet and at the outside loop neighbor to the 74th residue. Further, we have detected that the slight conformational change of the NFV binding pocket due to N88D mutation induces the

increase of hydrophobic contacts between NFV and the protease. The loss of the interaction between 74T and 88D would lower the constraint at 29D, 31T, and 74T, which results in the slight conformational change of the active site. Energetic analysis evidently indicates this increase of hydrophobicity. Consequently, NFV is stabilized by the increase of hydrophobic effects when N88D is acquired, while D30N/N88D destabilizes NFV by a large loss of electrostatic interaction. The reduction of the constraint might induce the compensation for the loss of replicative capacity resulting from D30N and keep the binding affinity with substrates, while the resistance against NFV is retained.

90L/M is also located at the helix region near the dimer interface, not at the active site. L90M mutants complexed with a substrate analogue inhibitor, not NFV, were also investigated by Mahalingam and co-workers.[14-16] They concluded that L90M altered van der Waals interactions in the hydrophobic interior at the dimer interface near the catalytic aspartates, and 90L related with the stability of the dimer. We also find the alteration of van der Waals interactions in the L90M model. Side chains of the 90th residues are close to the side chains of 24L/24'L and the main chain of 25D/25'D (Figure 7A). A methionine has a long and straight side chain, while a leucine has a diverging side chain. The substitution of methionine for leucine makes a collision of the 90th residues with 24L/24'L and 25D/25'D. This causes the conformational change at the triads. The conformational change of the triads induces large conformational changes at the flap and at the loop near the 79'P-81'P as a result of the presence of NFV (Figure 7B). Those regions are surprisingly very far apart from the 90th residue. In the L90M

Resistant Mechanism against NFV of HIV-1 PR

J. Phys. Chem. B, Vol. 109, No. 1, 2005 **573**

mutant, the conformation in the binding pocket is greatly changed. Specifically, the loop region moves outward from NFV and makes a large gap; therefore, the van der Waals and hydrophobic energies decrease greatly. The character of this conformational change resembles the conformational change of the indinavir-bound L90M protease[17] and the saquinavir-bound G48V/L90M protease.[57] The reason for the multidrug resistance relevant to the L90M mutation would be the conformational change of the triads, and, subsequently, these are hydrophobic at the flap and 79'P loop. The flap and loop region interact with each of the dodecahydroisoquinoline ring of NFV, the pyridyl group of indinavir, and the planar quinoline group of saquinavir. Those chemical bases are the largest in each inhibitor and are very bulky compared with the protease substrates. No structural distortion appears at the loop region of the L90M complexed with the substrate analogue inhibitors. Therefore, it is speculated that the structural distortion seen in the inhibitor-bound L90M mutants is due to the largeness of the quinoline ring or pyridyl group in volume. Then, to reduce or eliminate the resistance of L90M, the moiety that interacts with the loop region should be less bulky.

Our MD studies indicate that the drug-resistant mutations affect the conformations of the binding cavity and the hydrophilic and hydrophobic interactions at the active site, even though the location of mutated residues is apart from the active site.

Furthermore, the difference in the binding energy between the wild-type model and those of each mutant are compatible with the indices of resistance levels that were estimated from experimental IC90.[8,9] At present, there exist some computational approaches to explain the phenotype results.[32,35,58,59] Although each of them successfully predicted the decrease of the binding affinity in the case of the active site mutation, they failed in the prediction of the nonactive site mutation as L90M. Computational prediction is usually based on the assumption that PI resistance is primarily determined by a reduction in binding affinity. Therefore, the previous studies proposed that the drug resistance due to the nonactive site mutation might be caused by another mechanism, such as decreasing the dimer stability of the protease.[57,60] However, our study indicates that the assumption is applicable to the nonactive site mutation. Some nonactive site residues without any direct contact with inhibitors (e.g., 10L, 46M, and 90L) have a strong positional correlation with the residues located at the active site. Hence, the nonactive site mutations would cause a displacement of the active site residues and the decrease of the inhibitor or substrate binding affinity. We suggest that evaluating the positions of all the residues in the mutated protease is a key factor for the success in computational prediction of the protease resistivity against PIs. Additionally, it is also applicable to the design to reduce or to eliminate the resistance at the nonactive site mutations.

Conclusions

We executed MD simulations for the wild-type and D30N, N88D, D30N/N88D, and L90M mutants to clarify the resistant mechanism of each mutation against NFV. Our results could reproduce the phenotype data and clarified the conformational alterations at the active site and the interaction changes due to the mutation. D30N induces the disappearance of the hydrogen bond between the *m*-phenol group of NFV and the 30th residue, which results in the decrease of the electrostatic binding energy. Further, D30N loses the ability to retain a water molecule at the S2 pocket. N88D alters the conformation at the β sheets consisting of 74T and its vicinity greatly. N88D also affects

the active site conformation, which creates more favorable hydrophobic binding cavity. L90M affects the triads 25D26T27G and causes subsequent large conformational changes at the flap region and the 79'P loop, though the 90th residue is far apart from those regions. L90M decreases the van der Waals binding energy greatly.

Supporting Information Available: RMSD of the main chain atoms compared with the X-ray crystal structure (Figure 1S). This material is available free of charge via the Internet at http://pubs.acs.org.

References and Notes

(1) Kohl, N.E.; Emini, E. A.; Schleif, W. A.; Davis, L. J.; Heimbach, J. C.; Dixon, R. A.; Scolnick, E. M.; Sigal, I. S. *Proc. Natl. Acad. Sci. U.S.A.* **1988**, *85*, 4686.

(2) Debouck, C. *AIDS Res. Hum. Retroviruses* **1992**, *8*, 153.

(3) Roberts, N. A.; Martin, J. A.; Kinchington, D.; Broadhurst, A. V.; Craig, J. C.; Duncan, I. B.; Galpin, S. A.; Handa, B. K.; Kay, J.; Krohn, A.; Lambert, R. W.; Merrett, J. H.; Mills, J. S.; Parkes, K. E. B.; Redshaw, S.; Ritchie, A. J.; Taylor, D. L.; Thomas, G. J.; Machin, P. J. *Science* **1990**, *248*, 358.

(4) Johnson, V. A.; Brun-Vézinet, F.; Clotet, B.; Conway, B.; D'Aquila, R. T.; Demeter, L. M.; Kuritzkes, D. R.; Pillay, D.; Schapiro, J. M.; Telenti, A.; Richman, D. *Top. HIV Med.* **2003**, *11*, 215.

(5) Wu, T. D.; Schiffer, C. A.; Gonzales, M. J.; Taylor, J.; Kantor, R.; Chou, S.; Israelski, D.; Zolopa, A. R.; Fessel, W. J.; Shafer, R. W. *J. Virol.* **2003**, *77*, 4836.

(6) Kantor, R.; Fessel, W. J.; Zolopa, A. R.; Israelski, D.; Shulman, N.; Montoya, J. G.; Harbour, M.; Schapiro, J. M.; Shafer, R. W. *Antimicrob. Agents Chemother.* **2002**, *46*, 1086.

(7) Condra, J. H.; Schleif, W. A.; Blahy, O. M.; Gabryelski, L. J.; Graham, D. J.; Quintero, J. C.; Rhodes, A.; Robbins, H. L.; Roth, E.; Shivaprakash, M.; Titus, D.; Yang, T.; Teppler, H.; Squires, K. E.; Deutsch, P. J.; Emini, E. A. *Nature* **1995**, *374*, 569.

(8) Patick, A. K.; Duran, M.; Cao, Y.; Shugarts, D.; Keller, M. R.; Mazabel, E.; Knowles, M.; Chapman, S.; Kuritzkes, D. R.; Markowitz, M. *Antimicrob. Agents Chemother.* **1998**, *42*, 2637.

(9) Patick, A. K.; Mo, H.; Markowitz, M.; Appelt, K.; Wu, B.; Musick, L.; Kalish, V.; Kaldor, S.; Reich, S.; Ho, D.; Webber, S. *Antimicrob. Agents Chemother.* **1996**, *40*, 292 (Erratum, *40*, 1575).

(10) Jacobson, H.; Hängii, M.; Ott, M.; Duncan, I. B.; Owen, S.; Andreoni, M.; Vella, S.; Mous, J. *J. Infect. Dis.* **1996**, *173*, 1379.

(11) Sugiura, W.; Matsuda, Z.; Yokomaku, Y.; Hertogs, K.; Larder, B.; Oishi, T.; Okano, A.; Shiino, T.; Tatsumi, M.; Matsuda, M.; Abumi, H.; Takata, N.; Shirahata, S.; Yamada, K.; Yoshikura, H.; Nagai, Y. *Antimicrob. Agents Chemother.* **2002**, *46*, 708.

(12) Sugiura, W.; Oishi, T.; Okano, A.; Matsuda, M.; Abumi, H.; Yamada, K.; Koike, M.; Taki, M.; Ishikawa, M.; Miura, T.; Hukutake, K.; Gouchi, K.; Ajisawa, A.; Iwamoto, A.; Hanabusa, H.; Mimaya, J.; Takamatsu, J.; Takata, N.; Kakishita, E.; Higasa, S.; Kashiwagi, S.; Shirahata, A.; Nagai, Y. *Jpn. J. Infect. Dis.* **1999**, *52*, 175.

(13) Kaldor, S. W.; Kalish, V. J.; Davies, J. F.; Shetty, B. V.; Fritz, J. E.; Appelt, K.; Burgess, J. A.; Campanale, K. M.; Chirgadze, N. Y.; Clawson, D. K.; Dressman, B. A.; Hatch, S. D.; Khalil, D. A.; Kosa, M. B.; Lubbehusen, P. P.; Muesing, M. A.; Patick, A. K.; Reich, S. H.; Su, K. S.; Tatlock, J. H. *J. Med. Chem.* **1997**, *40*, 3979.

(14) Mahalingam, B.; Boross, P.; Wang, Y.-F.; Louis, J. M.; Fischer, C. C.; Tozser, J.; Harrison, R. W.; Weber, I. T. *Proteins* **2002**, *48*, 107.

(15) Mahalingam, B.; Louis, J. M.; Hung, J.; Harrison, R. W.; Weber, I. T. *Proteins* **2001**, *43*, 455.

(16) Mahalingam, B.; Louis, J. M.; Reed, C. C.; Adomat, J. M.; Krouse, J.; Wang, Y.-F.; Harrison, R. W.; Weber, I. T. *Eur. J. Biochem.* **1999**, *263*, 238.

(17) Mahalingam, B.; Wang, Y.-F.; Boross, P. I.; Tozser, J.; Louis, J. M.; Harrison, R. W.; Weber, I. T. *Eur. J. Biochem.* **2004**, *271*, 1516.

(18) Piana, S.; Bucher, D.; Carloni, P.; Rothlisberger, U. *J. Phys. Chem. B* **2004**, *108*, 11139.

(19) Piana, S.; Parrinello, M.; Carloni, P. *J. Mol. Biol.* **2002**, *319*, 567.

(20) Trylska, J.; Bala, P.; Geller, M.; Grochowski, P. *Biophys. J.* **2002**, *83*, 794.